I&EC research
Industrial & Engineering Chemistry Research
pubs.acs.org/IECR
Article

Determination of Kinetic and Diffusion Parameters Needed to Predict the Behavior of CaO-Based CO_2 Sorbent and Sorbent-Catalyst Materials

Andrea Di Giuliano, Katia Gallucci, and Pier Ugo Foscolo*

Cite This: https://dx.doi.org/10.1021/acs.iecr.9b05383
Read Online

ABSTRACT: For about 10 years, this research group has developed and utilized a particle grain model (PGM), to simulate CO_2-capture carried out by CaO-based porous particles. Chemical kinetics and diffusion parameters were either taken from literature studies or fixed by fitting experimental sorption data. As recently observed, this procedure was not fully satisfactory and revealed systematic, minor discrepancies between PGM numerical results and experimental data when predicting sorbents behavior during the initial chemically controlled regime of carbonation. This work deals with the experimental determination of kinetic and diffusion parameters, utilized in the PGM, by means of straightforward thermogravimetric analysis (TGA) tests on small samples of materials to be evaluated for CO_2 sorption and sorption-enhanced processes. To validate this procedure, the carbonation of two Ni−CaO−mayenite combined sorbent-catalyst materials (CSCMs) was studied in TGA. The experimental data so obtained were used to infer carbonation kinetic parameters tailored for each CSCM, which resulted to be compatible with investigated phenomena and previously proposed values, and allowed faithful PGM predictions at different operating temperatures. These parameters were then implemented in an axial dispersion plug flow reactor model for sorption enhanced steam methane reforming (SESMR): its predictions resulted in good agreement with experimental data from SESMR tests performed in packed beds.

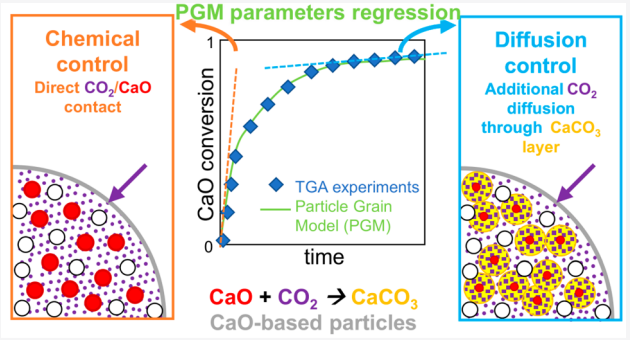

1. INTRODUCTION

Calcium oxide (CaO) has been considered as the most advantageous CO_2-sorbent within the mixed oxides family (Mg, Zn, Cu, K, Al, and Ca) because it carbonates (CBN, Reaction 1) over a wider range of adsorption temperatures (200−700 °C),[1] is easily available at a competitive price,[2,3] and is regenerated by calcination, even though it undergoes a strong reduction of sorption capacity under cyclic carbonation/calcination usage, because of sintering.[4−7] To face this issue, CaO is utilized in combined forms with inert stabilizers: dolomite is a natural material with this feature, while the literature refers to the synthetic CaO-based materials, with different inert phases (Al_2O_3 or calcium−aluminates $Ca_xAl_yO_z$ above all[2]).

$$\text{CBN:}\quad CaO_{(s)} + CO_{2(g)} \leftrightarrow CaCO_{3(s)}$$
$$\Delta H^0_{298K} = -175.7\ \text{kJ mol}^{-1} \qquad \text{(Reaction 1)}$$

In situ CO_2 separation, that is, capture of CO_2 simultaneously to its production, was proposed as a promising strategy,[8,9] applicable to chemical looping combustion of hydrocarbons,[10,11] gasification with calcium looping cycle,[12−15] steam reforming of methane (SMR, Reaction 2)[2,16−21] or higher hydrocarbons (SR, Reaction 3).[22−24] Besides the net reduction of CO_2 emissions, the in situ CO_2 capture brings in an additional advantage, known as "sorption-enhancing": the subtraction of CO_2 from the gaseous reaction environment displaces the equilibria of the water gas shift (WGS, Reaction 4) and then of steam reforming (Reaction 2, Reaction 3) toward products, therefore increasing outlet H_2 purity.

$$\text{SMR:}\quad CH_{4(g)} + H_2O_{(v)} \leftrightarrow CO_{(g)} + 3H_{2(g)}$$
$$\Delta H^0_{298K} = 206.2\ \text{kJ mol}^{-1} \qquad \text{(Reaction 2)}$$

$$\text{SR:}\quad C_nH_{m(g)} + nH_2O_{(v)} \leftrightarrow nCO_{(g)} + (n + m/2)H_{2(g)}$$
(Reaction

Special Issue: Carbon Capture and Utilization

Received: September 27, 2019
Revised: December 21, 2019
Accepted: January 31, 2020

$$\text{WGS:}\quad CO_{(g)} + H_2O_{(v)} \leftrightarrow CO_{2(g)} + H_{2(g)}$$
$$\Delta H^0_{298K} = -41.2\text{kJ mol}^{-1} \qquad \text{(Reaction 4)}$$

All this considered, exploitation of CaO as CO_2-sorbent appears as a versatile and promising practice to face the ever more urging issues related to climate change mitigation.[25−27] The effective application on a large scale needs experimental testing of efficient materials and technologies, as well as the refinement of modeling tools, in order to get reliable predictions of the CaO peculiar dynamic behavior in CBN (Reaction 1) processes. This work is focused on the latter field.

From the kinetic point of view, CBN (Reaction 1) occurs according to two subsequent regimes: (i) the first step is fast and controlled by the chemical reaction between CaO and CO_2 (chemically controlled regime), with "isles" of $CaCO_3$ nucleating on the CaO surface exposed to gaseous CO_2; (ii) the second is slower and occurs as CaO conversion increases, since the freshly produced layer of $CaCO_3$ entirely covers CaO still available, determining a predominant diffusion resistance for CO_2 to get in direct contact with CaO (diffusion-controlled regime).[2,4,28−31] This confers to the CaO conversion curve as a function of time the well-known knee-bended shape (initial steep straight line and final quasi-horizontal plateau joined by a rounded knee-bend).[30] Several modeling approaches have been conceived to describe this behavior: empirical models,[32,33] shrinking core models,[34,35] random pore models,[30,36−38] grain models,[39−41] ion reaction mechanism model,[42] and rate equation theory model.[31]

In the last 10 years, this research group was committed[43−47] in developing a particle grain model (PGM, among the so-called "grain models"), which simulates the carbonation behavior of CaO grains supported on an inert matrix, with an optional catalytic phase (in cases of further reactions to be performed simultaneously with CBN).

In that PGM, each particle is spherical, made in turn of spherical grains of inert phase and CaO separated by pores (particle void fraction ε_p); the optional, catalytically active phase is assumed as finely and uniformly dispersed on those grains. Such particles are exposed to an infinite expanse of a gaseous mixture containing CO_2, with constant composition ($C_{CO2,bulk}$): CO_2 diffuses through the pores, approaching the CaO grains surface, where CBN (Reaction 1) occurs developing a spherical shell of $CaCO_3$, adherent to each CaO shrinking core; that $CaCO_3$ product layer thickens as CaO conversion increases, being penetrated with greater resistance by CO_2 molecules, which are bound to react on the surface of each CaO shrinking core; as the product layer grows, ε_p progressively decreases, because of the ratio between $CaCO_3$ molar volume and that of CaO (ζ = 2.18; 36.9 cm^3 mol^{-1}, and 16.8 cm^3 mol^{-1}, respectively[48]).

Gallucci et al.[43] proposed the first version of PGM, for CBN (Reaction 1) taking place inside particles of calcined dolomite. Their PGM calculated CaO conversion as a function of time by two separated kinetic laws, respectively simulating the chemically- and diffusion-controlled regimes, with initial CaO grain diameter (δ^0_{CaO}) and CO_2 diffusivity through $CaCO_3$ product layer (D_{PL}) as fitting parameters, and using the kinetic constant for surface reaction (k_S) from Bhatia and Perlmutter.[30] Calculated CaO conversion fitted well experimental values from CO_2 capture tests in thermogravimetric analysis (TGA).

Stendardo and Foscolo[44] introduced a variable D_{PL} (as an exponential-decay function of CaO conversion, tuned by means of two numerical parameters, named a and b), in order to model the whole extent of CBN by a unique kinetic law, able to represent both regimes and the transition between them. They fitted well experimental CaO conversions recorded in TGA for dolomite samples, by imposing Bhatia and Perlmutter[30] kinetic constant k_S for the chemically controlled regime.

Aloisi et al.[45] expanded the PGM field of application, by combining the sorption functionality and some catalytic activity in a single bifunctional particle. They investigated combined sorbent-catalyst materials (CSCMs) made of CaO and nickel (Ni, SMR catalyst[49,50]) integrated with inert calcium-aluminates, developed for sorption enhanced steam methane reforming (SESMR, that is, the simultaneous occurring of Reaction 1, Reaction 2, and Reaction 4). They validated the PGM sorption functionality, by comparing simulations to experimental data from TGA multicycle carbonation/calcination tests: the progressive decay of CSCM sorption performance was well simulated by increasing δ^0_{CaO} cycle by cycle (mimicking sintering phenomena), while tuned a and b were kept constant for all cycles. In addition, they carried out a SESMR sensitivity study on CSCM particles, utilizing the PGM integrated with Numaguchi and Kikuchi[51] kinetic laws for SMR (Reaction 2) and WGS (Reaction 4).

Aloisi et al.[46] modeled purposely synthesized CSCMs, made of Ni and CaO supported on $Ca_{12}Al_{14}O_{33}$ (mayenite), and CaO-mayenite sorbents. As far as CBN (Reaction 1) is concerned, they obtained a good agreement between PGM outputs and experimental CaO conversion curves from TGA multicycle tests, using parameters δ^0_{CaO}, a, and b as done in the previous paper.[45] In addition, they[46] developed and validated an axial dispersion plug flow reactor (ADPFR) model to simulate SESMR carried out by a packed bed of a given CSCM: PGM kinetic equations were combined with molar balances for all gaseous species flowing through the packed bed.

Di Giuliano et al.[47] refined the PGM and ADPFR model to study the multicycle behavior of one optimized CSCM,[52] able to perform hundreds of SESMR/sorbent-regeneration cycles in a packed bed reactor: remarkably enough, at a given cycle number, the same parameters δ^0_{CaO}, a, and b,—as determined by PGM fitting of CaO conversion in TGA tests—were suitable for a faithful prediction of SESMR performance with the ADPFR model of a packed bed reactor.

However, Di Giuliano et al.[47] highlighted a minor bias in PGM predictions of TGA experimental CaO conversion as a function of time: notwithstanding the globally good agreement between simulations and experimental results, PGM systematically underestimated CaO conversion during the chemically controlled regime, with respect to corresponding TGA experimental data, while the diffusion-controlled step was always simulated more reliably; these discrepancies were attributed to the value of k_S taken from the literature,[30] without any adjustment to the behavior of the material at hand. Previous publications[43−46] also showed similar inconsistencies, even though globally good predictions were assured.

The chemically controlled regime of CBN (Reaction 1) is the most important step for practical applications, since the diffusion-controlled regime brings in carbonation rates far too low for industrial interest. Then, improving predictions of the chemically controlled regime is a relevant task.

https://dx.doi.org/10.1021/acs.iecr.9b05383
Ind. Eng. Chem. Res. XXXX, XXX, XXX−XXX

To this scope, this work proposes and validates a method suitable for CaO-based sorbents or CSCMs to experimentally determine tailored PGM parameters from TGA CO_2 capture tests. That method is applied to two Ni−CaO−mayenite CSCMs (developed in the framework of European research project ASCENT, G.A. 608512), tested in TGA at three temperature levels: these tailored parameters assured a remarkable improvement of the PGM fitting quality of TGA carbonation tests with respect to previous works. As a further validation, for both investigated CSCMs, the ADPFR model was able to predict the concentrations of H_2, CO, CO_2, and CH_4, at the exit of simulated packed bed reactors, in full agreement with experimental data taken from the literature[21] at a microreactor scale (0.5 g of packed bed), or purposely obtained in this work at a bench scale (6.8 g of packed bed).

2. MATERIALS AND METHODS

2.1. Experimental Section. *2.1.1. CSCMs Synthesis.* Two Ni−CaO−mayenite CSCMs were synthesized by the already validated sequence of wet mixing and wet impregnation methods, fully described elsewhere:[21,53] each CaO−mayenite sorbent produced by wet mixing (nominal 15 and 54 wt % free CaO, respectively) was impregnated to get a final 10 wt % of Ni content. From here on, the resulting CSCMs are named "CaO15Ni10" and "CaO54Ni10", respectively.

Detailed characterizations[52,54,55] assessed the effectiveness of the synthesis process in producing the desired CSCMs.

2.1.2. CSCM Characterization. Reliable physicochemical inputs were provided to models used in this work to simulate the behavior of each CSCM, on the basis of their experimental characterization.

X-ray diffraction (XRD) analyses (diffractometer Bruckner AXS D8 Advanced using Cu Kα radiation, Bragg angle from 20° to 70°, scanning step of 0.0158°, sampling time of 1 s per step) allowed estimating average CaO crystallite diameters of fresh CSCM (δ^{Sch}_{CaO}) by Scherrer equation.[56,57]

Particle porosities (i.e., void fraction) of calcined CSCMs were determined by GEOPYC 1360 and ACCUPYC 1330 devices, respectively, as done in reference 47.

2.1.3. CO_2-Capture TGA Tests. The device used for TGA tests was a Linseis STA PT1000 equipped with alumina crucibles. Long-term CO_2 capture tests at several CBN temperatures (T_{CBN} = 600, 650, or 700 °C) were performed on fresh samples of CaO15Ni10 and CaO54Ni10, as well as on Al_2O_3 (these last results were used as *blank*, reference values to correct the TGA raw measurements on CSCM materials). Instantaneous mass variation signal was recorded with a 0.2 Hz sampling frequency.

Each sample (30−40 mg, particle diameter in the range from 38 to 106 μm, to make negligible the influence of operating conditions[46]) underwent a preliminary treatment to desorb gases and decompose contingent $CaCO_3$ or $Ca(OH)_2$ due to exposure to ambient air. This treatment included 10 °C min^{-1} heating-ramp up to 850 °C, followed by 30 min dwell at 850 °C and cooling down to T_{CBN}, all under 230 NmL min^{-1} of N_2. Afterward, the sample was kept for 7 h at T_{CBN}, under 230 NmL min^{-1} of a gaseous mixture of 18 vol % of CO_2 in N_2 ($C_{CO2,bulk}$), so to carry out CBN (Reaction 1). This duration was assumed as sufficient to convert all the available CaO in $CaCO_3$, therefore the overall long-term mass increase with respect to sample mass at the end of preliminary treatment (Δm_{fin}) was representative of actual sorption capacity of the examined sample.[46,47,58]

Instantaneous mass increase ($\Delta m(t)$) with respect to sample mass recorded at the end of preliminary treatment was used to calculate CaO conversion as a function of time ($X(t)$, eq 1).

$$X(t) = \frac{\Delta m(t)}{\Delta m_{fin}} \tag{1}$$

2.1.4. SESMR test. CaO15Ni10 was tested for SESMR in a heated vertical bench-scale packed-bed reactor, fully described in previous works[47,52] (internal diameter of 1.57 cm, packed bed made of 6.8 g of CSCM, particle diameter in the range between 212 and 600 μm). The application of the Weisz-Prater[59] criterion allowed predicting a Ni catalyst effectiveness factor close to 1, for SMR at the experimental conditions. On the other hand, as far as CO_2 sorption is concerned, fluidized bed adsorption tests with calcined dolomite[60] showed that CaO dynamic conversion is affected very slightly by particle size up to 780 μm.

The packed bed was first prereduced in order to get Ni^0, the active phase in SMR catalysis: 150 NmL min^{-1} of a reducing gaseous stream (10 vol % of H_2 in N_2) were fed to the reactor, heated from room temperature to 900 °C by 10 °C min^{-1} heating-ramp, then kept at 900 °C for 30 min. Afterward, the reactor was cooled down to 650 °C, under a reducing stream of 150 NmL min^{-1} (5 vol % of H_2 in N_2).

SESMR followed, at 650 °C and 1 atm, with feeding gases including 27 NmL min^{-1} of CH_4, 100 NmL min^{-1} of N_2 and inlet steam to carbon molar ratio of 3. Measurements of overall outlet flow rate (cooled and dried) and of its composition allowed calculating flow rates of H_2, CH_4, CO, and CO_2 ($F_{i,out}$) and related concentrations on dry and dilution-free basis ($Y_{i,out}$, eq 2):

$$Y_{i,out} = \frac{F_{i,out}}{\sum_j F_{j,out}} 100; \quad i, j = CH_4, H_2, CO, CO_2 \tag{2}$$

2.2. Modeling. *2.2.1. Innovative Approach to Model CBN.* The starting point for mathematical modeling was the CBN (Reaction 1) local rate, already reported by Gallucci et al.[43] and Stendardo and Foscolo[44] (eq 3). That local rate was referred to the CaO grains surface by a shrinking core approach, using k_S defined as a kinetic constant for a surface reaction (see section S1 of Supporting Information [SI] for further details).

$$r_{CBN} = 6\left(\frac{k_S N^0_{CaO}}{\delta^0_{CaO}}\right) N^0_{CaO} V_{CaO} (1 - X)^{2/3} (C_{CO_2,c} - C_{CO_2,eq}) \tag{3}$$

Effects of CO_2 diffusion through the $CaCO_3$ product layer were then taken into account, describing diffusivity as an exponential-decay function of CaO conversion ($D_{PL}(X)$)[44] (the whole procedure is shown in Di Giuliano et al.[47]). This brought us to the final form of CBN kinetics for the PGM (eq 4) used in past works from this research group,[45−47] and expressed in terms of CO_2 molar concentation adjacent to the product layer, that is, inside the pores ($C_{CO2,s}$), instead of its value at the CaO core surface ($C_{CO2,c}$), as in eq 3.

$$r_{CBN} = \frac{3N^0_{CaO} V_{CaO} \left(\frac{k_S N^0_{CaO}}{\delta^0_{CaO}/2}\right) (1 - X)^{2/3} (C_{CO_2,s} - C_{CO_2,eq})}{1 + \frac{k_s N^0_{CaO}}{D_{PL}(X)} (\delta^0_{CaO}/2) \sqrt[3]{1 - X} \left(1 - \sqrt[3]{\frac{1 - X}{1 - X + \zeta X}}\right)} \tag{4}$$

https://dx.doi.org/10.1021/acs.iecr.9b05383
Ind. Eng. Chem. Res. XXXX, XXX, XXX−XXX

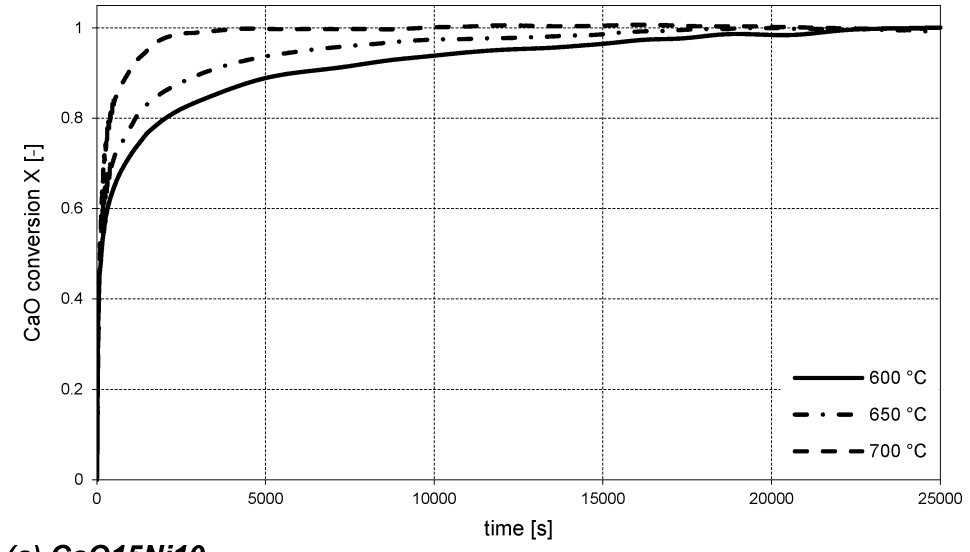

Figure 1. Experimental CaO conversion (X) in TGA CO_2 capture tests carried out on fresh samples of CaO15Ni10 (a) and CaO54Ni10 (b) at T_{CBN} = 600, 650, and 700 °C, respectively.

A rearrangement of eq 4 was here carried out, obtaining at the denominator the linear combination of two characteristic times, τ_{CBN} and $\tau_{PL}(X)$, associated with chemical- and diffusion-controlled regimes, respectively (eq 5).

$$\begin{cases} r_{CBN} = N^0_{CaO}\dfrac{3V_{CaO}(1-X)^{2/3}(C_{CO_2,s}-C_{CO_2,eq})}{\tau_{CBN}+\tau_{PL}(X)\sqrt[3]{1-X}\left(1-\sqrt[3]{\dfrac{1-X}{1-X+\zeta X}}\right)} \\ \tau_{CBN} = \left(\dfrac{k_S N^0_{CaO}}{\delta^0_{CaO}/2}\right)^{-1} = \left(\dfrac{k_{CBN}}{\delta^0_{CaO}/2}\right)^{-1} \\ \tau_{PL}(X) = \left(\dfrac{D_{PL}(X)}{(\delta^0_{CaO}/2)^2}\right)^{-1} \end{cases} \quad (5)$$

It is worth discussing the structure of τ_{CBN} and $\tau_{PL}(X)$ (eq 5), which respectively combine effects from local surface kinetics ($k_{CBN} = k_S\, N^0_{CaO}$) or product layer diffusion ($D_{PL}(X)$) with initial dimension of CaO grains ($\delta^0_{CaO}/2$). Their dependence on $\delta^0_{CaO}/2$ is formally correct, since it refers to the influence on CBN from actual CaO surface per unit sorbent volume exposed to incoming CO_2:[30] the larger is $\delta^0_{CaO}/2$, the lower is the actual CaO surface available for CBN (for a given N^0_{CaO}), and then the slower is the CBN process, that is, the higher is the relevant characteristic times. Anyway, the CaO specific surface is a very peculiar quantity, even for pure CaO samples (e.g., depending on pore properties and procedure of sample preparation[61]); its experimental estimation may turn out to be tricky in the case of sorbents made of other components in addition to CaO, as the CSCMs studied here.

In previous works from this research group,[43−47,58] k_S was assumed equal to 5.95 × 10^{-7} m^4 $kmol^{-1}$ s^{-1}, for all studied CaO-based sorbents; that value was determined experimentally

https://dx.doi.org/10.1021/acs.iecr.9b05383
Ind. Eng. Chem. Res. XXXX, XXX, XXX−XXX

by Bhatia and Perlmutter[30] on pure CaO samples obtained from limestone, the CaO specific surface of which was determined by mercury penetration porosimetry. The specific surface value was needed to get their kinetic constant per unit surface, k_S.

To model more accurately CBN and SESMR carried out by CSCM, it is convenient to determine experimentally, by means of quite simple measurements, the two functional groups appearing in the definition of τ_{CBN} and $\tau_{PL}(X)$, which incorporate all the mutual effects influencing the dynamics of CBN (Reaction 1) and may be specific for each tested material. In such a way, the arbitrary assumption of quantities, taken from different literature sources and related to other sorbents, is avoided.

In what follows, a procedure is proposed for the acquisition of τ_{CBN} and $\tau_{PL}(X)$ from CO_2 capture TGA tests.

2.2.2. Fast Initial Chemically Controlled Regime. The CaO molar balance for a given CaO-based porous sorbent material can be expressed in terms of CaO conversion (eq 6).

$$\frac{\partial X}{\partial t} = \frac{r_{CBN}}{N^0_{CaO}} \tag{6}$$

At the beginning of the CO_2 capture process by means of such a sorbent, CO_2 concentration at the active CaO grain surface coincides with that inside pores ($C_{CO2,c} \equiv C_{CO2,s}$), since no $CaCO_3$ product layer has formed yet on the whole active sorption surface. By implementing this assumption directly in eq 3, one obtains the kinetic law characterizing the fast initial chemically controlled regime of CBN (eq 7) and the related CaO molar balance (eq 8):

$$r_{CBN} = 3N^0_{CaO}\left(\frac{k_{CBN}}{\delta^0_{CaO}/2}\right)V_{CaO}(1-X)^{2/3}(C_{CO_2,s} - C_{CO_2,eq}) = 3\frac{N^0_{CaO}}{\tau_{CBN}}V_{CaO}(1-X)^{2/3}(C_{CO_2,s} - C_{CO_2,eq}) \tag{7}$$

$$\frac{\partial X}{\partial t} = 3\left(\frac{k_{CBN}}{\delta^0_{CaO}/2}\right)V_{CaO}(1-X)^{2/3}(C_{CO_2,s} - C_{CO_2,eq}) = 3\frac{V_{CaO}}{\tau_{CBN}}(1-X)^{2/3}(C_{CO_2,s} - C_{CO_2,eq}) \tag{8}$$

Equation 8 can be further manipulated when applied to fine CSCM particles studied in this work (d_p < 500 μm),[60] for which CO_2 diffusion offers negligible pore mass transfer resistances;[30,44,62] then, it is assumed that CO_2 concentration inside the particle pores is practically uniform and so approaches external bulk values ($C_{CO2,s} \approx C_{CO2,bulk}$). This implies that eq 8 can be treated as an ordinary differential equation and solved by separation of variables, obtaining the linearized eq 9:

$$\frac{1-\sqrt[3]{1-X}}{V_{CaO}(C_{CO_2,bulk} - C_{CO_2,eq})} = \left(\frac{k_{CBN}}{\delta^0_{CaO}/2}\right)t = \frac{t}{\tau_{CBN}} \tag{9}$$

Equation 9 was used in each TGA test, in order to determine values of the group $\left(\frac{k_{CBN}}{\delta^0_{CaO}/2}\right)$, that is, of τ_{CBN}, as the slope of the regression line of points

$$\left(t;\ \frac{1-\sqrt[3]{1-X}}{V_{CaO}(C_{CO_2,bulk} - C_{CO_2,eq})}\right)$$

obtained from TGA experimental data, for X < 0.4: this boundary value was fixed according to experimental $X(t)$ trends (Figure 1) obtained for CaO15Ni10 and CaO54Ni10; anyway, it may be different for other materials, without affecting the methodology proposed here.

2.2.3. Diffusion-Controlled Regime. CBN kinetic law specified for the diffusion-controlled regime (eq 10) was drawn by means of a CO_2 shell molar balance on the $CaCO_3$ product layer, as described in section S2 of SI. The related CaO molar balance, resulting from the substitution of eq 10 in eq 6, is shown in eq 11.

$$r_{CBN} = 3\left(\frac{D_{PL}(X)}{(\delta^0_{CaO}/2)^2}\right)N^0_{CaO}V_{CaO}(C_{CO_2,s} - C_{CO_2,c})\frac{\sqrt[3]{1-X+X\zeta}\cdot\sqrt[3]{1-X}}{\sqrt[3]{1-X+X\zeta} - \sqrt[3]{1-X}} = \frac{3}{\tau_{PL}(X)}N^0_{CaO}V_{CaO}(C_{CO_2,s} - C_{CO_2,c})\frac{\sqrt[3]{1-X+X\zeta}\cdot\sqrt[3]{1-X}}{\sqrt[3]{1-X+X\zeta} - \sqrt[3]{1-X}} \tag{10}$$

$$\frac{\partial X}{\partial t} = 3\left(\frac{D_{PL}(X)}{(\delta^0_{CaO}/2)^2}\right)V_{CaO}(C_{CO_2,s} - C_{CO_2,c})\frac{\sqrt[3]{1-X+X\zeta}\cdot\sqrt[3]{1-X}}{\sqrt[3]{1-X+X\zeta} - \sqrt[3]{1-X}} = \frac{3}{\tau_{PL}(X)}V_{CaO}(C_{CO_2,s} - C_{CO_2,c})\frac{\sqrt[3]{1-X+X\zeta}\cdot\sqrt[3]{1-X}}{\sqrt[3]{1-X+X\zeta} - \sqrt[3]{1-X}} \tag{11}$$

When applied to the fine CSCM particles investigated in this work, eq 11 can be simplified: for the same reasons discussed for chemically controlled regime (subsection 2.2.2), the CO_2 radial gradient inside the particle pores is negligible and $C_{CO2,s} \approx C_{CO2,bulk}$; furthermore, as product layer diffusion is the bottleneck of the whole CBN process in the considered regime, it is reasonable to suppose that the CBN reaction at the active CaO core surface is fast enough to establish conditions close to equilibrium, so $C_{CO2,c} \approx C_{CO2,eq}$. In such a way, CO_2 concentration gradient in eq 11 is approximated as a constant at a given temperature, leaving only explicit dependencies on X.

For a given value of CaO conversion, named $\bar{X}$, the simplified eq 11 can be rearranged (eq 12):

$$\left(\frac{D_{PL}(\bar{X})}{(\delta^0_{CaO}/2)^2}\right) = \frac{\left.\frac{\partial X}{\partial t}\right|_{X=\bar{X}}}{3V_{CaO}(C_{CO_2,bulk} - C_{CO_2,eq})\frac{\sqrt[3]{1-\bar{X}+\bar{X}\zeta}\cdot\sqrt[3]{1-\bar{X}}}{\sqrt[3]{1-\bar{X}+\bar{X}\zeta} - \sqrt[3]{1-\bar{X}}}} = \frac{1}{\tau_{PL}(\bar{X})} \tag{12}$$

Equation 12 was used for each TGA test, in order to determine the values of the group $\left(\frac{D_{PL}(X)}{(\delta^0_{CaO}/2)^2}\right)$, that is, of $\tau_{PL}(X)$, for chosen CaO conversion values ($\bar{X}$ = 0.4, 0.5, 0.6, 0.7, 0.8 0.8276, 0.9, 0.95; 0.8276 is the $\bar{X}$ value such that the ratio of cubic roots in eq 12 is equal to 1). The quantity $\left.\frac{\partial X}{\partial t}\right|_{X=\bar{X}}$ appearing in eq 12 was estimated as the slope of the regression line (least-squares method) obtained from the experimental $X(t)$ curve made of the 20-points neighborhood centered on the considered $\bar{X}$. Thanks to the high sampling frequency during TGA tests, those neighborhoods imply time intervals of about 100 s, relatively short when considering the very slow evolution of carbonation under the diffusion-controlled regime, then they were locally well-approximated by straight lines.

An exponential-decay law (eq 13) was assumed for $\left(\frac{D_{PL}(X)}{(\delta^0_{CaO}/2)^2}\right)$, agreeing to the hypothesis formulated in

https://dx.doi.org/10.1021/acs.iecr.9b05383
Ind. Eng. Chem. Res. XXXX, XXX, XXX−XXX

Stendardo and Foscolo,[44] with the preexponential factor fixed as the ratio $\left(\frac{D_{PL,0}}{(\delta_{CaO}^{Sch}/2)^2}\right)$, where $D_{PL,0}$ is equal to CO_2 effective gas diffusivity in N_2 (corresponding to $D_{CO2,eff}$ in Table S1 of the SI) inside completely calcined CSCM particles, at CBN equilibrium conditions for the considered T_{CBN}. $\delta_{CaO}^{Sch}/2$ is the CaO crystallite radius estimated by XRD analyses (1.45×10^{-8} m for CaO15Ni10 and 1.54×10^{-8} m for CaO54Ni10[54,55]).

$$\frac{D_{PL}(X)}{(\delta_{CaO}^{0}/2)^2} = \frac{D_{PL,0}}{(\delta_{CaO}^{Sch}/2)^2}\exp(-aX^b) = \frac{1}{\tau_{PL}(X)} \quad (13)$$

The exponential decay function provides a good interpolation of experimental data as a function of X, confirming the abrupt decrease of D_{PL} as soon as sorbent conversion reaches certain values, down to levels typical for solid phase diffusion, as supposed by Bhatia and Perlmutter[30] and later confirmed in the application of the PGM by Stendardo and Foscolo.[44]

Equation 13 was then manipulated to get eq 14, which was applied to points $\left(\bar{X}; \frac{D_{PL}(\bar{X})}{(\delta_{CaO}^{0}/2)^2}\right)$ obtained from the application of eq 12, in order to calculate parameters a and b by means of power-law regression (least-squares method).

$$\ln\left(\frac{D_{PL,0}}{(\delta_{CaO}^{Sch}/2)^2} \Big/ \frac{D_{PL}(X)}{(\delta_{CaO}^{0}/2)^2}\right) = aX^b \quad (14)$$

2.2.4. The Application of PGM to CBN. As a consequence of manipulations described in subsection 2.2.1, the PGM was updated to the form summarized in Table S1. By means of methods described in subsections 2.2.2 and 2.2.3, to be used preliminarily for simulations, this newly elaborated version of the PGM avoids any arbitrary choice in the assumption of parameters k_{CBN}, a, b, and δ_{CaO}^{0}, as done in previous publications.[44−47] These are now obtainable for each sorbent or sorbent-catalyst material by means of a standardized procedure applied to rather simple TGA tests, and allow predicting the behavior of the solid particles under carbonation process conditions, as shown in the Results and Discussion section.

Equations summarized in Table S1 were implemented in MATLAB and the resulting system was integrated by means of the "pdepe" tool. For each TGA test, CaO conversion as a function of time calculated by PGM was compared with corresponding TGA experimental measurements.

2.2.5. ADPFR Model for SESMR in a Packed Bed Reactor. To simulate SESMR carried out in packed bed reactors, an ADPFR model for SESMR was obtained by combining the updated PGM with molar balances in the gas flowing through a packed bed of solid particles and penetrating their pores, obtaining the system of equations reported in Table S2: (i) SMR (Reaction 2) and WGS (Reaction 4) were considered in that model by means of Numaguchi and Kikuchi's catalytic kinetics laws;[51] (ii) CSCM particles, constituting the active packed bed, were small enough to make composition gradients negligible around them[45] and inside their pores (Weisz-Prater criterion[59]); therefore the concentration value for each gaseous species at a given position and time instant is uniquely defined inside the packed bed;[46] (iii) Dankwerts closed−closed vessel boundary conditions were considered;[63] (iv) according to Di Giuliano and Pellegrino,[64] the assumption of constant superficial velocity is admissible because of the relevant inert dilution in the feeding stream.

With regard to CBN kinetics, the same parameters regressed for PGM from TGA experimental data were implemented in τ_{CBN} and $\tau_{PL}(X)$ of the ADPFR model: in the light of findings from Di Giuliano et al.,[47] these parameters are expected to provide a good prediction of products composition obtained at the reactor outlet.

Equations summarized in Table S2 were implemented in MATLAB, and the resulting system was integrated by means of the "pdepe" tool. Reactor outlet volumetric percentages of H_2, CO, CO_2, and CH_4 as functions of time ($Y_{i,out}$), calculated by ADPFR integration, were compared with corresponding experimental measurements.

2.2.6. Equilibria of Chemical Reactions. Equilibrium constants as functions of temperature for SMR (Reaction 2) and WGS (Reaction 4) were calculated as reported in Aloisi et al.[46] The equilibrium constant for CBN (Reaction 1), and then the equilibrium CO_2 concentration ($C_{CO2,eq}$), were calculated according to the equation by Stanmore and Gilot,[65] utilized in our previous works[43−47] as well.

3. RESULTS AND DISCUSSION

3.1. Experimental Results. Figure 1 shows experimental CaO conversion as a function of time (eq 1), calculated from

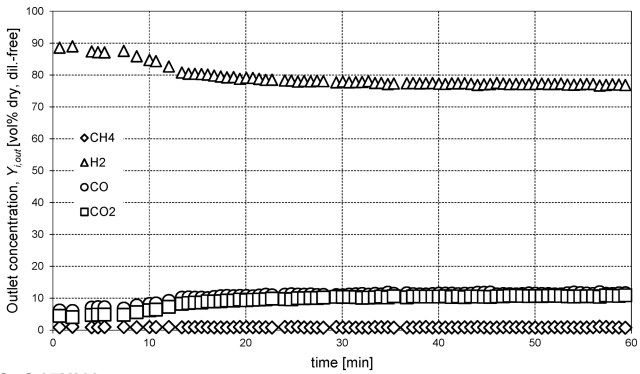

CaO15Ni10

Figure 2. Experimental outlet concentrations of CH_4, H_2, CO, CO_2 ($Y_{i,out}$) from the SESMR packed bed test on fresh CaO15Ni10 (650 °C, 1 atm).

Table 1. Results of $\left(\frac{k_{CBN}}{\delta_{CaO}^{0}/2}\right)$ Regressions by eq 9 from Experimental CaO Conversion Data from TGA CO_2 Capture Tests

	CaO15Ni10		CaO54Ni10	
T_{CBN} [°C]	$k_{CBN}/(\delta_{CaO}^{0}/2)$ [s^{-1}]	R^2	$k_{CBN}/(\delta_{CaO}^{0}/2)$ [s^{-1}]	R^2
600	83.1	0.960	59.4	0.947
650	82.7	0.967	59.4	0.981
700	82.9	0.993	51.7	0.928

data recorded during TGA CO_2-capture tests on fresh samples of CaO15Ni10 and CaO54Ni10, at T_{CBN} equal to 600, 650, and 700 °C, respectively.

All experimental CO_2 capture curves in Figure 1 show the typical knee-bended shape related to two different regimes of carbonation;, therefore, the PGM is suitable to model their CaO conversion versus time trends.

With both CSCMs, the increase of T_{CBN} involved the occurrence of knee-bending at higher X, that is, of the "switch

https://dx.doi.org/10.1021/acs.iecr.9b05383
Ind. Eng. Chem. Res. XXXX, XXX, XXX−XXX

Table 2. Results of $\left.\frac{\partial X}{\partial t}\right|_{X=\bar{X}}$ Regressions and of eq 12 for $\left(\frac{D_{PL}(\bar{X})}{(\delta^0_{CaO}/2)^2}\right)$ Calculations, from Experimental CaO Conversion Data Obtained in TGA CO_2 Capture Tests on CaO15Ni10

	CaO15Ni10								
	T_{CBN} = 600 °C			T_{CBN} = 650 °C			T_{CBN} = 700 °C		
$\bar{\bar{X}}$ [-]	$\left.\frac{\partial X}{\partial t}\right\|_{X=\bar{X}}$ [s^{-1}]	R^2	$\frac{D_{PL}(\bar{X})}{(\delta^0_{CaO}/2)^2}$ [s^{-1}]	$\left.\frac{\partial X}{\partial t}\right\|_{X=\bar{X}}$ [s^{-1}]	R^2	$\frac{D_{PL}(\bar{X})}{(\delta^0_{CaO}/2)^2}$ [s^{-1}]	$\left.\frac{\partial X}{\partial t}\right\|_{X=\bar{X}}$ [s^{-1}]	R^2	$\frac{D_{PL}(\bar{X})}{(\delta^0_{CaO}/2)^2}$ [s^{-1}]
0[a]			5.38×10^9			5.54×10^9			5.69×10^9
0.4	2.53×10^{-3}	0.994	6.19×10^0	4.35×10^{-3}	0.986	1.17×10^1	5.60×10^{-3}	0.986	1.80×10^1
0.5	8.54×10^{-4}	0.996	2.75×10^0	1.48×10^{-3}	0.989	5.25×10^0	3.46×10^{-3}	0.961	1.46×10^1
0.6	3.26×10^{-4}	0.999	1.35×10^0	5.27×10^{-4}	0.402	2.41×10^0	2.13×10^{-3}	0.956	1.17×10^1
0.7	1.24×10^{-4}	0.999	6.70×10^{-1}	2.90×10^{-4}	0.984	1.72×10^0	8.53×10^{-4}	0.900	6.06×10^0
0.8	5.18×10^{-5}	0.999	3.76×10^{-1}	1.31×10^{-4}	0.999	1.05×10^0	3.77×10^{-4}	0.715	3.60×10^0
0.8276	3.40×10^{-5}	0.999	2.71×10^{-1}	6.09×10^{-5}	0.999	5.35×10^{-1}	2.99×10^{-4}	0.740	3.15×10^0
0.9	1.05×10^{-5}	0.999	1.15×10^{-1}	3.00×10^{-5}	0.999	3.60×10^{-1}	1.26×10^{-4}	0.999	1.82×10^0
0.95	5.02×10^{-6}	0.999	7.74×10^{-2}	1.07×10^{-5}	0.999	1.81×10^{-1}	7.79×10^{-5}	0.999	1.59×10^0

[a]Preexponential factors $\left(\frac{D_{PL,0}}{(\delta^{Sch}_{CaO}/2)^2}\right)$, calculated as described in subsection 2.2.3.

Table 3. Results of $\left.\frac{\partial X}{\partial t}\right|_{X=\bar{X}}$ Regressions and of eq 12 for $\frac{D_{PL}(\bar{X})}{(\delta^0_{CaO}/2)^2}$ Calculations, from Experimental CaO Conversion Data Obtained in TGA CO_2-Capture Tests on CaO54Ni10

	CaO54Ni10								
	T_{CBN} = 600 °C			T_{CBN} = 650 °C			T_{CBN} = 700 °C		
$\bar{\bar{X}}$ [−]	$\left.\frac{\partial X}{\partial t}\right\|_{X=\bar{X}}$ [s^{-1}]	R^2	$\frac{D_{PL}(\bar{X})}{(\delta^0_{CaO}/2)^2}$ [s^{-1}]	$\left.\frac{\partial X}{\partial t}\right\|_{X=\bar{X}}$ [s^{-1}]	R^2	$\frac{D_{PL}(\bar{X})}{(\delta^0_{CaO}/2)^2}$ [s^{-1}]	$\left.\frac{\partial X}{\partial t}\right\|_{X=\bar{X}}$ [s^{-1}]	R^2	$\frac{D_{PL}(\bar{X})}{(\delta^0_{CaO}/2)^2}$ [s^{-1}]
0[a]			4.36×10^9			4.48×10^9			4.61×10^9
0.4	4.65×10^{-3}	0.975	$1.1.4 \times 10^1$	2.83×10^{-3}	0.969	7.61×10^0	1.40×10^{-3}	0.983	4.51×10^0
0.5	7.43×10^{-4}	0.975	2.39×10^0	3.95×10^{-4}	0.964	1.40×10^0	4.52×10^{-4}	0.997	1.92×10^0
0.6	1.79×10^{-4}	0.940	7.45×10^{-1}	1.52×10^{-4}	0.935	6.90×10^{-1}	2.18×10^{-4}	0.975	1.19×10^0
0.7	6.10×10^{-5}	0.999	3.29×10^{-1}	9.44×10^{-5}	1.000	5.59×10^{-1}	1.37×10^{-4}	0.769	9.72×10^{-1}
0.8	3.00×10^{-5}	0.999	2.17×10^{-1}	3.53×10^{-5}	0.999	2.82×10^{-1}	5.02×10^{-5}	0.999	4.80×10^{-1}
0.8276	2.63×10^{-5}	0.999	2.10×10^{-1}	2.78×10^{-5}	1.000	2.44×10^{-1}	4.03×10^{-5}	0.999	4.24×10^{-1}
0.9	1.03×10^{-5}	0.998	1.13×10^{-1}	1.33×10^{-5}	0.999	1.60×10^{-1}	2.00×10^{-5}	0.999	2.88×10^{-1}
0.95	1.02×10^{-5}	0.996	1.58×10^{-2}	8.52×10^{-6}	0.999	1.45×10^{-1}	9.34×10^{-6}	0.999	1.34×10^{-1}

[a]Preexponential factors $\left(\frac{D_{PL,0}}{(\delta^{Sch}_{CaO}/2)^2}\right)$, calculated as described in subsection 2.2.3.

Table 4. Arrhenius Parameters for $\left(\frac{D_{PL}(\bar{X})}{(\delta^0_{CaO}/2)^2}\right)$ with $\bar{X}$ = 0.8 and 0.9, i.e., in the Fully Developed Diffusion-Controlled Regime

		CaO15Ni10		CaO54Ni10	
		$\bar{X}$ = 0.8	$\bar{X}$ = 0.9	$\bar{X}$ = 0.8	$\bar{X}$ = 0.9
A	[s^{-1}]	1.20×10^9	4.36×10^{10}	4.35×10^2	9.62×10^2
E_{PL}	[kJ mol^{-1}]	159.2	194.2	55.5	66.0

region" from one regime to the other; this is in agreement with the experimental findings of Bhatia and Perlmutter.[30] CaO15Ni10 (Figure 1a) showed a clearer distinction between chemically- and diffusion-controlled regimes than CaO54Ni10 (Figure 1b), the higher T_{CBN} the more emphasized this effect appeared; this peculiarity of CSCM behavior confirms the need of procedures as that proposed in this work to get tailored modeling parameters.

In addition, when the time scale is sufficiently expanded, the initial very short sigmoid shape noticed ibidem and attributed to nucleation[30] also takes place. As mentioned in section 2.1.3, TGA tests were carried out at operating conditions not affecting sorbent conversion dynamics, so that the assignment of such behavior to an intrinsic feature of the material is convincing, more than the assignment to the gas flow dispersion phenomena in the analytical equipment at the start of the sorption step.

Figure 2 shows the experimental results of the SESMR test with a bench scale packed bed made of CaO15Ni10 small particles. On the whole, the behavior (Figure 2) substantially confirms what was observed in previous works on the same material.[47,52] Thanks to sorption enhancing due to CBN (Reaction 1), initial H_2 and CO_2 outlet concentrations were respectively higher (88 vol % dry, dilution-free) and lower (5 vol % dry, dilution-free) than SMR (Reaction 2) equilibrium values at 650 °C and 1 atm, that is, 77.0 vol % of H_2, 10.7 vol

https://dx.doi.org/10.1021/acs.iecr.9b05383
Ind. Eng. Chem. Res. XXXX, XXX, XXX−XXX

Table 5. Parameter Values Assumed for PGM Simulations

	CaO15Ni10			CaO54Ni10		
Process and Physical Parameters:						
temp, T_{CBN} [°C]	600	650	700	600	650	700
pressure, P [atm]	1	1	1	1	1	1
CO_2 molar fraction in the gaseous bulk, $C_{CO2,bulk}$ [vol %]	18	18	18	18	18	18
average particle diameter, d_p [μm]	72	72	72	72	72	72
Initial particle void fraction, ε_p^0 [−]	0.42	0.42	0.42	0.45	0.45	0.45
Model Parameters:						
$\frac{1}{\tau_{CBN}} = \frac{k_{CBN}}{\delta_{CaO}^0/2}$ [s^{-1}]	82.9	82.9	82.9	56.8	56.8	56.8
$\frac{D_{PL,0}}{(\delta_{CaO}^{Sch}/2)^2}$ [s^{-1}]	5.38×10^9	5.54×10^9	5.69×10^9	4.36×10^9	4.48×10^9	4.61×10^9
a	24.869	23.903	21.946	24.896	24.547	23.960
b	0.217	0.204	0.144	0.231	0.192	0.160
α [−][60,67]	1.65	1.65	1.65	1.65	1.65	1.65

% of CO_2, dry and dilution-free basis.[21] As the sorbent phase became progressively saturated, the sorption-enhancing effect vanished causing a breakthrough, with $Y_{i,out}$ progressively changing and finally leveling to values close to those of SMR thermodynamic equilibrium (0.8 vol % of CH_4, 77.0 vol % of H_2, 11.5 vol % of CO and 10.7 vol % of CO_2, on dry and dilution-free basis[21]).

Only CaO15Ni10 was considered for the packed bed SESMR test at the bench-scale under the ASCENT research project, since it was known to ensure the full catalytic activity for SMR, thanks to its lower CaO/Ni ratio,[21] foreseeing long-term SESMR applications.[47]

As far as CaO54Ni10 is concerned, microreactor scale experimental SESMR results were taken from Di Giuliano et al.,[21] for ADPFR model validation in this work.

3.2. Modeling Results and Validation. *3.2.1. Regression of CBN Kinetic Parameters Utilizing TGA Data.* As far as the fast chemically controlled regime is concerned, eq 9 and the related regression method (subsection 2.2.2) were applied to the initial points of experimental CaO conversion ($X(t) < 0.4$), for each of six CO_2 capture tests carried out in TGA (CaO15Ni10 and CaO54Ni10, each tested at three temperature levels).

Results are summarized in Table 1 (see also Figure S1 of SI). Overall, the quality of regressed $\left(\frac{k_{CBN}}{\delta_{CaO}^0/2}\right)$ is acceptable, as shown by coefficients of determination (R^2 in Table 1), confirming the suitability of eq 9 to the aim of this work. For each CSCM, variations of T_{CBN} do not cause relevant changes in $\left(\frac{k_{CBN}}{\delta_{CaO}^0/2}\right)$ (Table 1), in full agreement with findings from Bhatia and Perlmutter[30] on pure CaO samples. As a consequence, a unique average value of $\left(\frac{k_{CBN}}{\delta_{CaO}^0/2}\right)$ was assumed for each CSCM on the whole temperature range 600−700 °C: 82.9 s^{-1} for CaO15Ni10 and 56.8 s^{-1} for CaO54Ni10, corresponding to τ_{CBN} of 1.21×10^{-2} s and 1.77×10^{-2} s, respectively. An estimation of related k_S was carried out by means of the τ_{CBN} definition in eq 5, in which N_{CaO}^0 is known from the respective nominal CaO content and a good approximation of $\delta_{CaO}^0/2$ magnitude is offered by $\delta_{CaO}^{Sch}/2$ values. The values 2.83×10^{-7} m^4 $kmol^{-1}$ s^{-1} and 7.57×10^{-8} m^4 $kmol^{-1}$ s^{-1} resulted for CaO15Ni10 and CaO54Ni10, respectively. These are in fair agreement with the experimental results of Bhatia and Permutten,[30] with their value of 5.95×10^{-7} m^4 $kmol^{-1}$ s^{-1} for k_S: in their Figures 3 and 4,[30] CaO samples reached CaO conversion of 0.5 in about 0.4 min at temperatures close to T_{CBN} used in TGA tests of this work, while the same conversion level occurred between 1.5 and 2 min for CaO15Ni10 and between 2 and 4 min for CaO54Ni10, respectively. As a matter of fact, the smaller k_S values found here with respect to Bhatia and Permutten[30]'s findings agree quite well with the somewhat longer time interval needed by both CSCMs to reach 0.5 CaO conversion. This further correspondence corroborated the reliability of the proposed method for $\left(\frac{k_{CBN}}{\delta_{CaO}^0/2}\right)$ estimation.

With regard to the diffusion-controlled regime, the regression method described in subsection 2.2.3 was applied to the latter part of the experimental CaO conversion curves from TGA tests ($X(t) \geq 0.4$).

As a first step local slopes were obtained by linear regression, then used in eq 12 to calculate $\left(\frac{D_{PL}(\bar{X})}{(\delta_{CaO}^0/2)^2}\right)$. Results are summarized in Table 2 for CaO15Ni10 and in Table 3 for CaO54Ni10: a general good quality of regressions emerged, with some exceptions due to occasional TGA signal fluctuations around the clear trend of the CaO conversion curve, anyway always centered on the regression lines.

Three comments were suggested by the results in Table 2 and Table 3, which corroborated the proposed method for estimation of $\left(\frac{D_{PL}(X)}{(\delta_{CaO}^0/2)^2}\right)$, from the physicochemical point of view: (i) by assuming an order of magnitude of 10^{-8} m for δ_{CaO}^0 (in agreement with reported Scherrer average diameters of CaO crystallites), calculated values of $\left(\frac{D_{PL}(\bar{X})}{(\delta_{CaO}^0/2)^2}\right)$ gave an estimation of particle layer diffusivity $D_{PL}(X)$ with orders of magnitude ranging between 10^{-15} m^2 s^{-1} and 10^{-19} m^2 s^{-1}, comparable with solid phase diffusivities, as already noticed in the literature,[30] compatible with the modeled phenomenon of CO_2 diffusion through $CaCO_3$ shells; (ii) $\left(\frac{D_{PL}(\bar{X})}{(\delta_{CaO}^0/2)^2}\right)$, and then $D_{PL}(X)$, was described as a decreasing function of X; (iii) for both samples, characteristic times at high CaO conversion $\tau_{PL}(X \geq 0.9)$ are lower than respective τ_{CBN} by 2 or 3 orders of magnitude, as expected because of the reduced rate of CBN diffusion-controlled regime with respect to the chemically controlled one.

https://dx.doi.org/10.1021/acs.iecr.9b05383
Ind. Eng. Chem. Res. XXXX, XXX, XXX−XXX

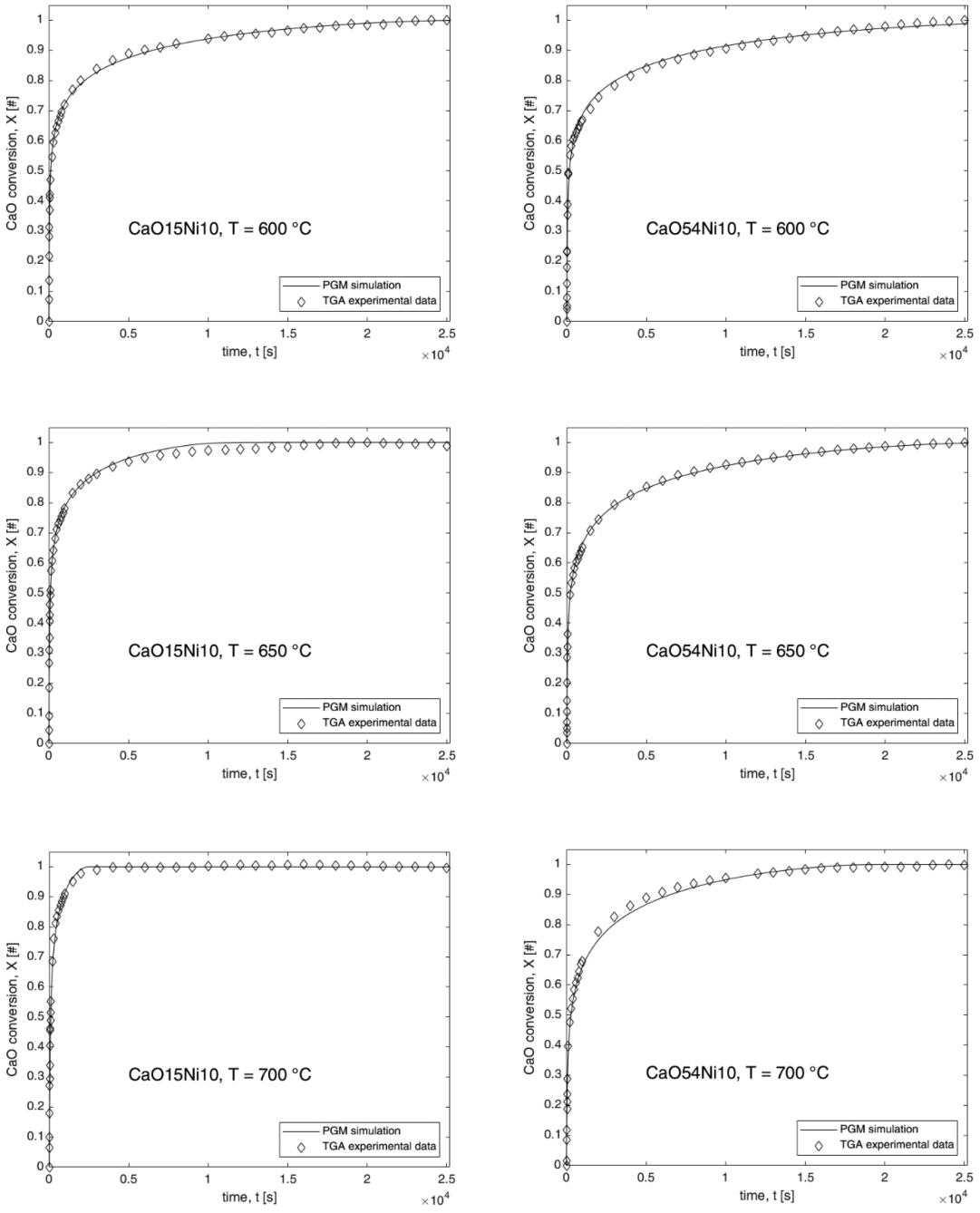

Figure 3. Experimental data of CO_2 capture TGA tests and corresponding PGM simulations of CaO conversion (X) as a function of time.

The series of $\left(\frac{D_{PL}(\overline{X})}{(\delta^0_{CaO}/2)^2}\right)$ values (Table 2 and Table 3) from each TGA test were then set in eq 14, used to infer by power-law regression the parameters a and b of exponential-decay defined in eq 13 (Figure S2 of the SI).

In addition, $\left(\frac{D_{PL}(\overline{X})}{(\delta^0_{CaO}/2)^2}\right)$ regressed for $\overline{X}$ = 0.8 and 0.9 at the three T_{CBN} temperature levels were used to get pre-exponential (A) and activation energy (E_{PL}) parameters of the related Arrhenius-type function (Table 4). The above CaO conversion values were chosen as they assured the complete development of the diffusion-controlled regime. In Table 4, the activation energies of CaO15Ni10 agreed with those obtained by López et al. (CaO−mayenite sorbents, 177 kJ mol^{-1}),[62] Bhatia and Perlmutter (CaO from limestone samples above 515 °C, 179.2 kJ mol^{-1}),[30] Grasa et al. (CaO from limestone samples, 163 kJ mol^{-1}),[38] while those of CaO54Ni10 were closer to results from Zou et al. (CaO−$Ca_9Al_6O_{18}$ sample with 80 wt % of CaO, 88.7 kJ mol^{-1}).[66] López et al.[62] found a constant diffusion activation energy for many samples of CaO-based sorbents with different CaO content, although the related pre-exponential factor changed according to each sample.

3.2.2. PGM Simulations of CBN. Table 5 contains all experimental and modeling input values used in PGM to simulate CO_2-capture TGA tests on CaO15Ni10 and CaO54Ni10; these include CBN kinetic parameters regressed in the subsection 3.2.1.

As a whole, very good agreement resulted between PGM predictions of CaO conversion path and experimental data obtained in long-duration TGA tests, as shown on Figure 3:

https://dx.doi.org/10.1021/acs.iecr.9b05383
Ind. Eng. Chem. Res. XXXX, XXX, XXX−XXX

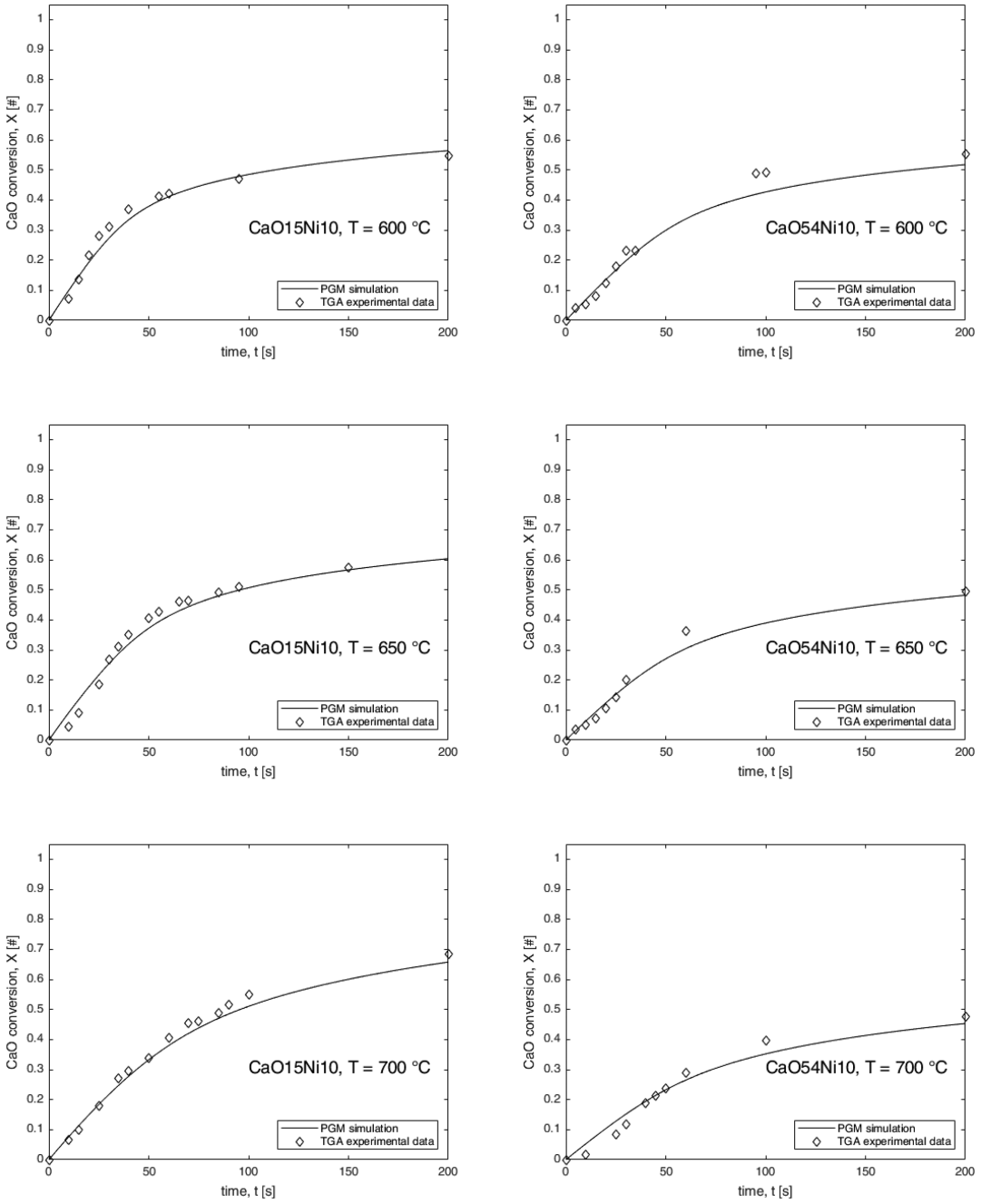

Figure 4. Experimental data of CO_2 capture TGA tests and corresponding PGM simulations of CaO conversion (X) as a function of time: initial trends reproduced on a magnified time scale with respect to Figure 3.

this confirms the validity of the PGM model developed by this research group and testifies to the accuracy of the novel procedure described in subsections 2.2.2 and 2.2.3 to determine CBN parameters related to chemically- and diffusion-controlled regimes.

The calculated intraparticle profiles of CO_2 concentration highlighted that pore diffusional resistances are negligible for the investigated case of study (Figure S3), as expected for particles smaller than about 500 μm.[60]

It should be stressed here that the TGA experimental data shown in Figure 1 and Figure 3 were preliminarily utilized to determine the characteristic time in the chemically- and diffusion-controlled regimes. However, each characteristic time was obtained considering a subset of the experimental CaO conversion and a purposely drawn equation: the subset concerning the very beginning of CaO conversion and eq 7, on one hand, and that characterized by $X(t) \geq 0.4$ and eq 10, on the other hand. The comprehensive carbonation rate equation of PGM (eq 5), used here to obtain predictions of the typical knee-bended shape of the CaO conversion curve in its full extent, was not utilized in the determination of parameters for chemically- and diffusion-controlled regimes.

With regard to the issues mentioned in the Introduction, the quality of PGM/TGA fitting was also observed in more detail for the initial CaO conversion trend as a function of time (Figure 4): the PGM formulation proposed in this work (Table S1) and the experimental determination of CBN kinetic parameters, tailored for each sorbent material (subsections

https://dx.doi.org/10.1021/acs.iecr.9b05383
Ind. Eng. Chem. Res. XXXX, XXX, XXX−XXX

Table 6. 8. Experimental Input Values for Simulations with the ADPFR Model

	CaO15Ni10 bench-scale packed bed	CaO54Ni10 microreactor packed bed
temp, T_{CBN} [°C]	650	650
pressure, P [atm]	1	1
CH_4 inlet, $F_{CH4,in}$ [NmL min^{-1}]	27	2
N_2 inlet, $F_{N2,in}$ [NmL min^{-1}]	100	2
Ar inlet, $F_{Ar,in}$ [Nml min^{-1}]	0	10
inlet molar steam/carbon [−]	3	3
average particle diameter, d_p [μm]	406	112.5
initial particle void fraction, ε_p^0 [−]	0.42	0.45
bed diameter, d_b [cm]	1.57	0.70
bed mass, m_b [g]	6.8	0.5
packed bed void fraction, ε_b [−]	0.5	0.5

Table 7. Model Parameters Assumed in ADPFRD Model Simulations

	CaO15Ni10 bench-scale packed bed	CaO54Ni10 microreactor packed bed
axial dispersion coefficient, D_R [$m^2\ s^{-1}$]	2.5×10^{-3}	5.0×10^{-4}
$\frac{1}{\tau_{CBN}} = \frac{k_{CBN}}{\delta_{CaO}^0/2}$, [$s^{-1}$]	82.9	56.8
$\frac{D_{PL,0}}{(\delta_{CaO}^{Sch}/2)^2}$ [s^{-1}]	5.54×10^9	4.48×10^9
a	23.903	24.547
b	0.204	0.192
α [−][60,67]	1.65	1.65

2.2.2 and 2.2.3), allowed reaching a noticeable accuracy in fitting experimental sorption data, superior to that obtained previously for the same CSCM (Di Giuliano et al.[47]), specifically more accurate predictions of chemically controlled CaO conversion and of its knee-bending, that is, the regions of maximum interest in practical applications. Figure 4 also shows the initial sigmoidal shape affecting the experimental carbonation conversion trend in the first very few seconds, already mentioned and discussed in section 3.1.

3.2.3. ADPFR Model Simulations. Table 6 shows all experimental input values used in the ADPFR model (Table S2) to simulate a SESMR process carried out at 650 °C in a bench-scale tubular reactor filled with a CaO15Ni10 packed bed, and in a microreactor filled with a CaO54Ni10 packed bed.[21] CBN kinetic parameters, regressed for CaO15Ni10 and CaO54Ni10 from TGA tests at 650 °C (subsection 3.2.1), were part of model parameters assumed for the same simulations (Table 7).

Figure 5 shows the comparison between experimental outlet concentrations from the SESMR tests ($Y_{i,out}$) and corresponding ADPFR model outputs. A reliable prediction of the experimental results was obtained for SESMR tests in the packed bed reactor, at both scales and with both CSCMs.

ADPFR model predicted well the presence of some CO_2 and CO in the reactor outlet stream since the beginning of both tests, found experimentally. This indicates that the whole packed bed was involved in the CO_2 capture process since the beginning of tests, which is reasonable for such small-size reactors operating at the experimental gas hourly space velocity of about 820 h^{-1} and with the D_R values reported in Table 7. ADPFR correctly calculated this, as resulting X at the end of CaO15Ni10 and CaO54Ni10 packed beds ($z^* = 1$) was greater than zero since the first simulated instants.

These results about packed bed reactors at different scales provided a thorough validation of the procedure to derive CBN parameters of chemically- and diffusion-controlled regimes from TGA experimental data.

4. CONCLUSIONS

This work provided a significant step forward in the simulation of the CO_2 capture dynamic behavior of solid sorbents and combined sorbent-catalyst materials (CSCMs) by means of the particle grain model (PGM) proposed and utilized by this research group.

The proposed description of the carbonation rate successfully improved the PGM ability to predict CO_2 capture performances of CaO-based porous particles, thanks to the new approach based on characteristic times of chemically and diffusion-controlled regimes. The procedure was validated by means of the experimental and modeling study on two CSCMs; it is quite general and applicable to a multiplicity of CaO-based CO_2 sorbents and sorbent-catalyst materials.

CaO molar balances were derived for both regimes, obtaining two independent equations, in agreement with PGM interpretation of carbonation. For each material, those equations allowed determining chemically and diffusion-controlled characteristic times only from straightforward experimental measurements of CO_2 capture in TGA tests. The main features of those parameters were (i) inclusion of dependence on CaO specific surface, which avoided the need of its experimental determination, often affected by ambiguities in the case of composite materials; (ii) removal of arbitrary assumptions when defining fitting parameters of the carbonation kinetic law, with respect to previous applications of PGM.

The procedure to regress numerical values of parameters from TGA data was demonstrated to be sufficiently robust, as confirmed by coefficients of determination globally close to one, and able to provide results compatible to the investigated phenomena and to other literature studies on a similar subject: for each TGA test, the characteristic time for the chemically controlled regime was lower than the corresponding one for diffusion-control at relatively high CaO conversion values; estimated kinetic constants for surface reaction in the temperature range 600−700 °C resulted in fair agreement with those proposed elsewhere; estimated diffusivities of CO_2 through the the $CaCO_3$ product layer were comparable with those expected for solid-state diffusivities, and their temperature dependence found experimentally revealed activation energy values in fair agreement with those proposed in previous studies.

The PGM, with the implementation of experimentally determined kinetic parameters, provided very reliable predictions of CaO conversion as a function of time in TGA CO_2-capture tests, for both materials studied here, over the full extent of carbonation, and at all tested temperatures. Noticeably, numerical predictions were very accurate even in the initial part controlled by the chemical reaction rate, and at the beginning of diffusion-controlled regime (knee-bending of CaO conversion trend vs time); this result marks a relevant

https://dx.doi.org/10.1021/acs.iecr.9b05383
Ind. Eng. Chem. Res. XXXX, XXX, XXX−XXX

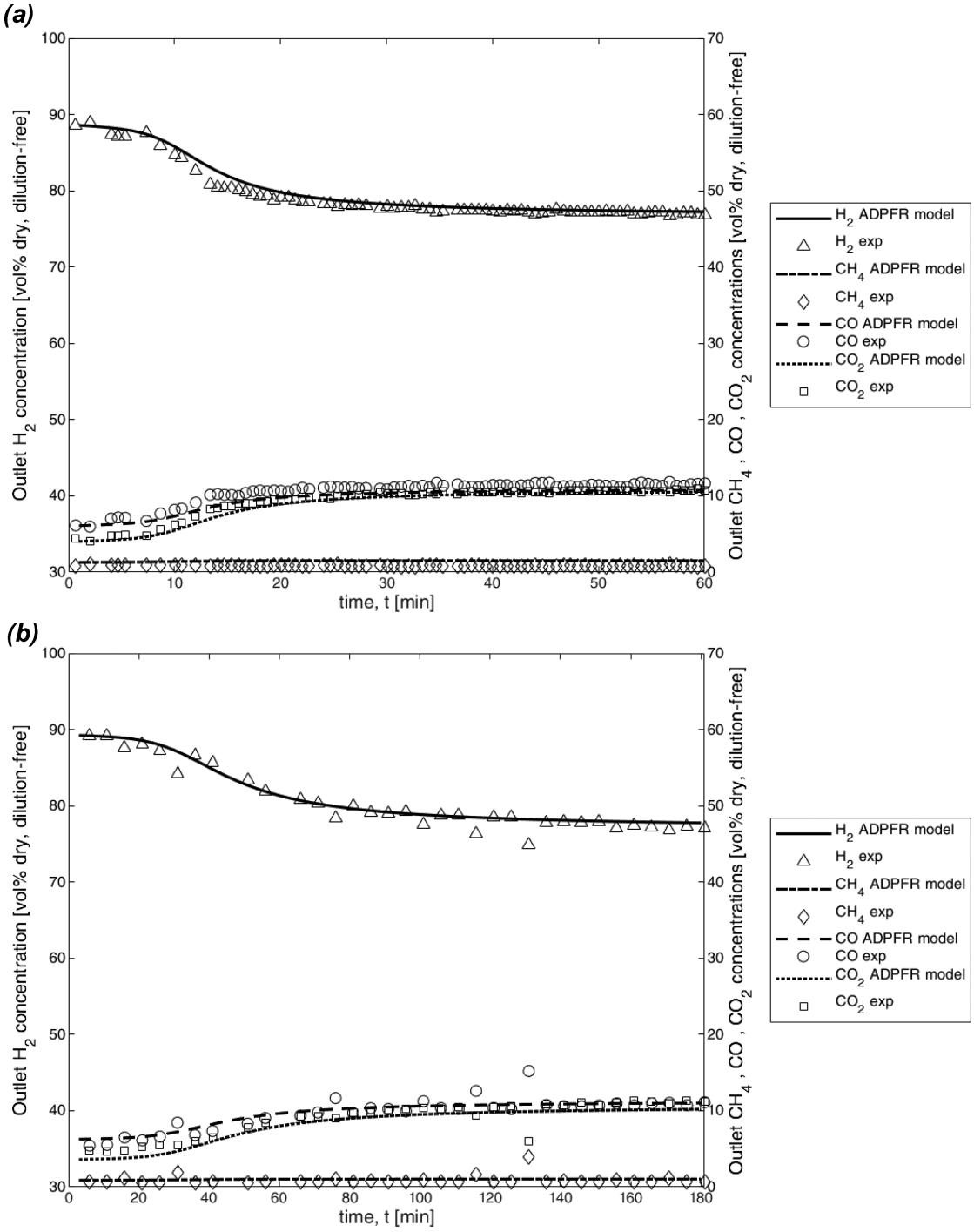

Figure 5. Experimental reactor outlet concentrations vs time (data points) from SESMR tests and ADPFR model simulations (lines) utilizing kinetic parameter values obtained from TGA: bench-scale SESMR test on CaO15Ni10 (a); microreactor test on CaO54Ni10, data from Di Giuliano et al.[21] (b).

improvement with respect to former applications of PGM proposed by this research team.

Last but not least, PGM carbonation kinetic law—with experimentally inferred parameters for both regimes—was implemented in an ADPFR model: SESMR experimental data, on two packed bed reactor scales and both CSCMs, and corresponding ADPFR model outputs resulted in fair agreement, offering a convincing validation of the approach proposed in this work.

It is worth mentioning here that finding tailored values for characteristic times of chemically- and diffusion-controlled regimes does not invalidate the approach, proposed in a previous paper,[47] to model sorption decaying (i.e., sintering increasing), which often affects the behavior of SESMR reactors under cyclic carbonation/calcination operating conditions. As it was done before, the newly proposed model parameters are obtainable by means of preliminary TGA tests, repeated on the same sample of the CaO-based material at hand, and then suitable to predict the performance of

https://dx.doi.org/10.1021/acs.iecr.9b05383
Ind. Eng. Chem. Res. XXXX, XXX, XXX−XXX

multicycle carbonation/calcination steps, which is the most likely application mode in continuous CO_2 sorption and sorption-enhanced processes at the industrial scale (e.g., high-purity H_2 production by means of SESMR processes in a packed bed and dual circulating fluidized bed reactors).

■ ASSOCIATED CONTENT

Supporting Information

The Supporting Information is available free of charge at https://pubs.acs.org/doi/10.1021/acs.iecr.9b05383.

Local kinetic law for CBN; CBN kinetic law in diffusion-controlled regime; complete sets of equations, boundary and initial conditions for PGM and ADPFR model; regressions of PGM parameters; intraparticle profiles from PGM simulations (PDF)

■ AUTHOR INFORMATION

Corresponding Author

Pier Ugo Foscolo − *University of L'Aquila, Department of Industrial and Computer Engineering and Economics, L'Aquila 67100, Italy*; orcid.org/0000-0002-0429-8487; Phone: +39 0862 434214; Email: pierugo.foscolo@univaq.it

Authors

Andrea Di Giuliano − *University of L'Aquila, Department of Industrial and Computer Engineering and Economics, L'Aquila 67100, Italy*

Katia Gallucci − *University of L'Aquila, Department of Industrial and Computer Engineering and Economics, L'Aquila 67100, Italy*

Complete contact information is available at: https://pubs.acs.org/10.1021/acs.iecr.9b05383

Notes

The authors declare no competing financial interest.

■ ACKNOWLEDGMENTS

The authors warmly thank Giampaolo Antonelli and Fabiola Ferrante (University of L'Aquila) for their help with experimental procedures, as well as Dr. Claire Courson for allowing the use of XRD and porosimetry devices at University of Strasbourg.

■ ABBREVIATIONS

ADPFR = Axial Dispersion Plug Flow Reactor
CBN = Carbonation
CCS = Carbon Capture and Storage
CSCM = Combined Sorbent-Catalyst Material(s)
GHG = GreenHouse-Gases
IPCC = United Nations Intergovernmental Panel on Climate Change
PGM = Particle Grain Model
SEM = Scanning Electron Microscopy
SESMR = Sorption-Enhanced Steam Methane Reforming
SI = Supporting Information
SMR = Steam Methane Reforming
SR = Steam Reforming
TGA = Thermogravimetric Analysis
WGS = Water Gas Shift
XRD = X-ray Diffraction

Symbols

a = parameter in exponential-decay of particle layer diffusivity, dimensionless
A = pre-exponential factor in Arrhenius-type function for product layer diffusivity, s^{-1}
b = parameter in exponential-decay of particle layer diffusivity, dimensionless
C = molar concentration, vol % or kmol m^{-3}
D = molecular diffusion coefficient, $m^2\ s^{-1}$
d_p = particle diameter, m
D_{PL} = product layer diffusivity coefficient, $m^2\ s^{-1}$
D_R = packed bed axial dispersion coefficient, $m^2\ s^{-1}$
D_{Knu} = Knudsen diffusivity, $m^2\ s^{-1}$
E = activation energy, J mol^{-1}
F = molar flow rate, kmol s^{-1}
h = mass transfer coefficient, m s^{-1}
H = height of the active packed bed, m
k_S = kinetic constant for the surface reaction, $m^4\ kmol^{-1}\ s^{-1}$
K_{SMR} = equilibrium constant for SMR reaction, atm^2
k_{SMR} = kinetic constant of SMR reaction, kmol $kg^{-1}\ s^{-1}\ atm^{0.404}$
K_{WGS} = equilibrium constant for WGS reaction, dimensionless
k_{WGS} = kinetic constant of WGS reaction, kmol $kg^{-1}\ s^{-1}\ atm^{-1}$
m = mass, kg
N_{CaO} = CaO moles per unit particle volume, kmol m^{-3}
P = pressure, atm
p = partial pressure, atm
R = radius, m
$\mathfrak{R}$ = ideal gas constant, J $mol^{-1}\ K^{-1}$
R^2 = coefficient of determination
r = particle radial coordinate, m
r_{CBN} = rate of CBN reaction, kmol $m^3\ s^{-1}$
r_{SMR} = rate of SMR reaction, kmol $kg^{-1}\ s^{-1}$
r_{WGS} = rate of WGS reaction, kmol $kg^{-1}\ s^{-1}$
S_b = packed bed reactor cross-sectional area, m^2
T = temperature, K
t = time, s
u = superficial velocity, m s^{-1}
V = molar volume, $m^3\ kmol^{-1}$
X = sorbent conversion, dimensionless
$X(t)$ = sorbent conversion as a function of time, dimensionless
Y = molar fraction on dry and dilution-free basis, vol % dry, dilution-free
z = reactor axial coordinate, m

Greek Letters

α = parameter in effective diffusivity, dimensionless
Δ = Difference, *initial−final quantity*
δ_{CaO} = CaO grain diameter, m
ε = packed bed voidage, dimensionless
ε_p = internal particle voidage, dimensionless
ζ = $CaCO_3$/CaO molar volume ratio, dimensionless
ν_{ij} = stoichiometric coefficient of species i in reaction j, $kmol_i$ per kmol of reference species
ρ = density, kg m^{-3}
σ_{CaO} = CaO grain surface per unit particle volume, m^{-1}
τ = characteristic time, s

Subscripts and superscripts

0 = initial
b = packed bed

https://dx.doi.org/10.1021/acs.iecr.9b05383
Ind. Eng. Chem. Res. XXXX, XXX, XXX−XXX

c = CaO core surface
CBN = carbonation
eff = effective
eq = equilibrium
fin = final
G = grain
in = inlet
out = outlet
p = particle
PL = product layer
por = pores
s = $CaCO_3$ shell external surface
Sch = Scherrer
tot = total
* = dimensionless

REFERENCES

(1) Gupta, H.; Fan, L. S. Carbonation-Calcination Cycle Using High Reactivity Calcium Oxide for Carbon Dioxide Separation from Flue Gas. *Ind. Eng. Chem. Res.* **2002**, *41* (16), 4035−4042.

(2) Shokrollahi Yancheshmeh, M.; Radfarnia, H. R.; Iliuta, M. C. High Temperature CO_2 Sorbents and Their Application for Hydrogen Production by Sorption Enhanced Steam Reforming Process. *Chem. Eng. J.* **2016**, *283*, 420−444.

(3) Feng, B.; An, H.; Tan, E. Screening of CO_2 Adsorbing Materials for Zero Emission Power Generation Systems. *Energy Fuels* **2007**, *21* (2), 426−434.

(4) Abanades, J. C.; Alvarez, D. Conversion Limits in the Reaction of CO_2 with Lime. *Energy Fuels* **2003**, *17* (2), 308−315.

(5) Blamey, J.; Anthony, E. J.; Wang, J.; Fennell, P. S. The Calcium Looping Cycle for Large-Scale CO2 Capture. *Prog. Energy Combust. Sci.* **2010**, *36* (2), 260−279.

(6) Grasa, G. S.; Abanades, J. C. CO_2 Capture Capacity of CaO in Long Series of Carbonation/Calcination Cycles. *Ind. Eng. Chem. Res.* **2006**, *45* (26), 8846−8851.

(7) Lysikov, A. I.; Salanov, A. N.; Okunev, A. G. Change of CO_2 Carrying Capacity of CaO in Isothermal Recarbonation-Decomposition Cycles. *Ind. Eng. Chem. Res.* **2007**, *46* (13), 4633−4638.

(8) Mahishi, M. R.; Goswami, D. Y. An Experimental Study of Hydrogen Production by Gasification of Biomass in the Presence of a CO_2 Sorbent. *Int. J. Hydrogen Energy* **2007**, *32* (14), 2803−2808.

(9) Florin, N. H.; Harris, A. T. Mechanistic Study of Enhanced H_2 Synthesis in Biomass Gasifiers with in-Situ CO_2 Capture Using CaO. *AIChE J.* **2008**, *54* (4), 1096−1109.

(10) Mattisson, T.; García-Labiano, F.; Kronberger, B.; Lyngfelt, A.; Adánez, J.; Hofbauer, H. Chemical-Looping Combustion Using Syngas as Fuel. *Int. J. Greenhouse Gas Control* **2007**, *1* (2), 158−169.

(11) Qiao, C.; Xiao, Y.; Xu, X.; Zhao, L.; Tian, W. Comparative Analysis of Hydrogen Production Systems from Biomass Based on Different Absorbent Regeneration Processes. *Int. J. Hydrogen Energy* **2007**, *32* (1), 80−85.

(12) Florin, N. H.; Harris, A. T. Preparation and Characterization of a Tailored Carbon Dioxide Sorbent for Enhanced Hydrogen Synthesis in Biomass Gasifiers. *Ind. Eng. Chem. Res.* **2008**, *47*, 2191.

(13) Harrison, D. P. Sorption-Enhanced Hydrogen Production: A Review. *Ind. Eng. Chem. Res.* **2008**, *47* (17), 6486−6501.

(14) Xie, X.; Li, Y.-J.; Liu, C.-T.; Wang, W.-J. HCl Absorption by $CaO/Ca_3Al_2O_6$ Sorbent from CO_2 Capture Cycles Using Calcium Looping. *Fuel Process. Technol.* **2015**, *138*, 500−508.

(15) Criado, Y. A.; Arias, B.; Abanades, J. C. Calcium Looping CO_2 Capture System for Back-up Power Plants. *Energy Environ. Sci.* **2017**, *10* (9), 1994−2004.

(16) Martavaltzi, C. S.; Pampaka, E. P.; Korkakaki, E. S.; Lemonidou, A. A. Hydrogen Production via Steam Reforming of Methane with Simultaneous CO2. *Energy Fuels* **2010**, *33* (4), 2589−2595.

(17) Martavaltzi, C. S.; Pefkos, T. D.; Lemonidou, A. A. Operational Window of Sorption Enhanced Steam Reforming of Methane over $CaO-Ca_{12}Al_{14}O_{33}$. *Ind. Eng. Chem. Res.* **2011**, *50* (2), 539−545.

(18) Cesário, M. R.; Barros, B. S.; Zimmermann, Y.; Courson, C.; Melo, D. M. A.; Kiennemann, A. CO_2 Sorption Enhanced Steam Reforming of Methane Using $Ni/CaO \cdot Ca_{12}Al_{14}O_{33}$ Catalysts. *Adv. Chem. Lett.* **2013**, *1* (3), 292−299.

(19) García-Lario, A. L.; Aznar, M.; Martinez, I.; Grasa, G. S.; Murillo, R. Experimental Study of the Application of a NiO/NiAl$_2$O < sub > 4 < 7sub> Catalyst and a CaO-Based Synthetic Sorbent on the Sorption Enhanced Reforming Process. *Int. J. Hydrogen Energy* **2015**, *40* (1), 219−232.

(20) García-Lario, A. L.; Grasa, G. S.; Murillo, R. Performance of a Combined CaO-Based Sorbent and Catalyst on H_2 Production, via Sorption Enhanced Methane Steam Reforming. *Chem. Eng. J.* **2015**, *264*, 697−705.

(21) Di Giuliano, A.; Girr, J.; Massacesi, R.; Gallucci, K.; Courson, C. Sorption Enhanced Steam Methane Reforming by Ni−CaO Materials Supported on Mayenite. *Int. J. Hydrogen Energy* **2017**, *42* (19), 13661−13680.

(22) Zamboni, I.; Courson, C.; Kiennemann, A. Synthesis of Fe/CaO Active Sorbent for CO_2 Absorption and Tars Removal in Biomass Gasification. *Catal. Today* **2011**, *176* (1), 197−201.

(23) D'Orazio, A.; Di Carlo, A.; Dionisi, N.; Dell'Era, A.; Orecchini, F. Toluene Steam Reforming Properties of CaO Based Synthetic Sorbents for Biomass Gasification Process. *Int. J. Hydrogen Energy* **2013**, *38* (30), 13282−13292.

(24) Zamboni, I.; Zimmermann, Y.; Kiennemann, A.; Courson, C. Improvement of Steam Reforming of Toluene by CO_2 Capture Using Fe/CaO e $Ca_{12}Al_{14}O_{33}$ Bi-Functional Materials. *Int. J. Hydrogen Energy* **2015**, *40* (15), 5297−5304.

(25) Pachauri, R. K.; Allen, M. R.; Barros, V. R.; Broome, J.; Cramer, W.; Christ, R.; Church, J. A.; Clarke, L.; Dahe, Q.; Dasgupta, P.; et al. *Climate Change 2014: Synthesis Report. Contribution of Working Groups I, II and III to the Fifth Assessment Report of the Intergovernmental Panel on Climate Change*. IPCC; Geneva, Switzerland; 2014 151 pp, ISBN 978-92-9169-143-2.

(26) Miller, D. C.; Litynski, J. T.; Brickett, L. A.; Morreale, B. D. Toward Transformational Carbon Capture Systems. *AIChE J.* **2016**, *62* (1), 2−10.

(27) COP 24 Katowice 2018. United Nations Climate Change Conference. https://cop24.gov.pl/ (accessed 2019-04-19).

(28) Dou, B.; Wang, C.; Song, Y.; Chen, H.; Jiang, B.; Yang, M.; Xu, Y. Solid Sorbents for In-Situ CO_2 Removal during Sorption-Enhanced Steam Reforming Process: A Review. *Renewable Sustainable Energy Rev.* **2016**, *53*, 536−546.

(29) Li, Z.; Liu, Y.; Cai, N. Understanding the Enhancement Effect of High-Temperature Steam on the Carbonation Reaction of CaO with CO_2. *Fuel* **2014**, *127*, 88−93.

(30) Bhatia, S. K.; Perlmutter, D. D. Effect of the Product Layer on the Kinetics of the CO_2-Lime Reaction. *AIChE J.* **1983**, *29* (1), 79−86.

(31) Li, Z. S.; Sun, H.; Cai, N. Rate Equation Theory for the Carbonation Reaction of CaO with CO_2. *Energy Fuels* **2012**, *26* (7), 4607−4616.

(32) Lee, D. K. An Apparent Kinetic Model for the Carbonation of Calcium Oxide by Carbon Dioxide. *Chem. Eng. J.* **2004**, *100* (1−3), 71−77.

(33) Li, Z. S.; Cai, N. S. Modeling of Multiple Cycles for Sorption-Enhanced Steam Methane Reforming and Sorbent Regeneration in Fixed Bed Reactor. *Energy Fuels* **2007**, *21* (5), 2909−2918.

(34) Szekely, J.; Evans, J. W. Studies in Gas-Solid Reactions: Part I. A Structural Model for the Reaction of Porous Oxides with a Reducing Gas. *Metall. Trans. 2* **1971**, No. 6, 1691−1698.

(35) Johnsen, K.; Ryu, H. J.; Grace, J. R.; Lim, C. J. Sorption-Enhanced Steam Reforming of Methane in a Fluidized Bed Reactor with Dolomite as CO_2 -Acceptor. *Chem. Eng. Sci.* **2006**, *61*, 1195−1202.

https://dx.doi.org/10.1021/acs.iecr.9b05383
Ind. Eng. Chem. Res. XXXX, XXX, XXX−XXX

(36) Bhatia, S. K.; Perlmutter, D. D. A Random Pore Model for Fluid-Solid Reactions: I. Isothermal, Kinetic Control. *AIChE J.* **1980**, *26* (3), 379−386.
(37) Bhatia, S. K.; Perlmutter, D. D. A Random Pore Model for Fluid-Solid Reactions: II. Diffusion and Transport Effects. *AIChE J.* **1981**, *27* (2), 247−254.
(38) Grasa, G.; Murillo, R.; Alonso, M.; Abanades, J. C. Application of the Random Pore Model to the Carbonation Cyclic Reaction. *AIChE J.* **2009**, *55* (5), 1246−1255.
(39) Heesink, A. B. M.; Prins, W.; van Swaaij, W. P. M. A Grain Size Distribution Model for Non-Catalytic Gas Solid Reactions. *Chem. Eng. J. Biochem. Eng. J.* **1993**, *53* (1), 25−37.
(40) Liu, W.; Dennis, J. S.; Sultan, D. S.; Redfern, S. A. T.; Scott, S. A. An Investigation of the Kinetics of CO_2 Uptake by a Synthetic Calcium Based Sorbent. *Chem. Eng. Sci.* **2012**, *69* (1), 644−658.
(41) Yu, Y. S.; Liu, W. Q.; An, H.; Yang, F. S.; Wang, G. X.; Feng, B.; Zhang, Z. X.; Rudolph, V. Modeling of the Carbonation Behavior of a Calcium Based Sorbent for CO_2 Capture. *Int. J. Greenhouse Gas Control* **2012**, *10*, 510−519.
(42) Wu, S. F.; Lan, P. Q. A Kinetic Model of Nano-CaO Reactions with CO_2 in a Sorption Complex Catalyst. *AIChE J.* **2012**, *58* (5), 1570−1577.
(43) Gallucci, K.; Stendardo, S.; Foscolo, P. U. CO2 Capture by Means of Dolomite in Hydrogen Production from Syn Gas. *Int. J. Hydrogen Energy* **2008**, *33* (12), 3049−3055.
(44) Stendardo, S.; Foscolo, P. U. Carbon Dioxide Capture with Dolomite: A Model for Gas−Solid Reaction within the Grains of a Particulate Sorbent. *Chem. Eng. Sci.* **2009**, *64* (10), 2343−2352.
(45) Aloisi, I.; Jand, N.; Stendardo, S.; Foscolo, P. U. Hydrogen by Sorption Enhanced Methane Reforming: A Grain Model to Study the Behavior of Bi-Functional Sorbent-Catalyst Particles. *Chem. Eng. Sci.* **2016**, *149*, 22−34.
(46) Aloisi, I.; Di Giuliano, A.; Di Carlo, A.; Foscolo, P. U.; Courson, C.; Gallucci, K. Sorption Enhanced Catalytic Steam Methane Reforming: Experimental Data and Simulations Describing the Behaviour of Bi-Functional Particles. *Chem. Eng. J.* **2017**, *314*, 570.
(47) Di Giuliano, A.; Gallucci, K.; Giancaterino, F.; Courson, C.; Foscolo, P. U. Multicycle Sorption Enhanced Steam Methane Reforming with Different Sorbent Regeneration Conditions: Experimental and Modelling Study. *Chem. Eng. J.* **2019**, *377*, 119874.
(48) Robie, R. A.; Bethke, P. M.; Beardsley, K. M. X-Ray Crystallographic Data, Molar Vol.s, and Densities of Minerals and Related Substances. In *Handbook of Chemistry and Physics*; Weast, R. C., Ed.; The Chemical Rubber Co.: Cleveland, OH, 1969; p B-308.
(49) Broda, M.; Manovic, V.; Imtiaz, Q.; Kierzkowska, A. M.; Anthony, E. J.; Müller, C. R. High-Purity Hydrogen via the Sorption-Enhanced Steam Methane Reforming Reaction over a Synthetic CaO-Based Sorbent and a Ni Catalyst. *Environ. Sci. Technol.* **2013**, *47* (11), 6007−6014.
(50) Barelli, L.; Bidini, G.; Gallorini, F.; Servili, S. Hydrogen Production through Sorption-Enhanced Steam Methane Reforming and Membrane Technology: A Review. *Energy* **2008**, *33* (4), 554−570.
(51) Numaguchi, T.; Kikuchi, K. Intrinsic Kinetics and Design Simulation in a Complex Reaction Network; Steam-Methane Reforming. *Chem. Eng. Sci.* **1988**, *43* (8), 2295−2301.
(52) Di Giuliano, A.; Giancaterino, F.; Courson, C.; Foscolo, P. U.; Gallucci, K. Development of a Ni-CaO-Mayenite Combined Sorbent-Catalyst Material for Multicycle Sorption Enhanced Steam Methane Reforming. *Fuel* **2018**, *234*, 687−699.
(53) Di Giuliano, A.; Courson, C.; Gallucci, K.; Kiennemann, A. *Ni-CaO Combined Sorbent-Catalyst Materials Usage for Sorption Enhanced Steam Methane Reforming*. In WHEC 2016, 21st World Hydrogen Energy Conference 2016, Proceedings 2016; Spanish Hydrogen Association (AeH2), 2016; pp 68−70.
(54) Di Giuliano, A. *Synthesis, Characterization and Industrial Applicability of Combined Sorbent-Catalysts Materials for Sorption Enhanced Steam Methane Reforming*. Ph.D. Thesis, University of L'Aquila-University of Strasbourg, 2017.
(55) Di Giuliano, A.; Gallucci, K.; Foscolo, P. U.; Courson, C. Effect of Ni Precursor Salts on Ni-Mayenite Catalysts for Steam Methane Reforming and on Ni-CaO-Mayenite Materials for Sorption Enhanced Steam Methane Reforming. *Int. J. Hydrogen Energy* **2019**, *44* (13), 6461−6480.
(56) Monshi, A.; Foroughi, M. R.; Monshi, M. R. Modified Scherrer Equation to Estimate More Accurately Nano-Crystallite Size Using XRD. *World J. Nano Sci. Eng.* **2012**, *02* (03), 154−160.
(57) Langford, J. I.; Wilson, A. J. C. Scherrer after Sixty Years: A Survey and Some New Results in the Determination of Crystallite Size. *J. Appl. Crystallogr.* **1978**, *11* (2), 102−113.
(58) Di Giuliano, A.; Aloisi, I.; Jand, N.; Foscolo, P. U.; Courson, C.; Gallucci, K. Sorption Enhanced Steam Methane Reforming: Experimental Data and Simulations Describing the Behaviour of Bi-Functional Particles. In WHEC 2016, 21st World Hydrogen Energy Conference 2016, Proceedings; Spanish Hydrogen Association (AeH2), 2016; Vol. *1*, pp 111−113.
(59) Weisz, P. B.; Prater, C. D. Interpretation of Measurements in Experimental Catalysis. *Adv. Catal.* **1954**, *6*, 143−196.
(60) Stendardo, S.; Di Felice, L.; Gallucci, K.; Foscolo, P. U. CO_2 Capture with Calcined Dolomite: The Effect of Sorbent Particle Size. *Biomass Convers. Biorefin.* **2011**, *1* (3), 149−161.
(61) Lu, H.; Reddy, E. P.; Smirniotis, P. G. Calcium Oxide Based Sorbents for Capture of Carbon Dioxide at High Temperatures. *Ind. Eng. Chem. Res.* **2006**, *45* (11), 3944−3949.
(62) López, J. M.; Grasa, G.; Murillo, R. Evaluation of the Effect of Inert Support on the Carbonation Reaction of Synthetic CaO-Based CO_2 Sorbents. *Chem. Eng. J.* **2018**, *350*, 559−572.
(63) Fogler, H. S. *Elements of Chemical Reaction Engineering*; Prentice Hall, 2005.
(64) Di Giuliano, A.; Pellegrino, E. Numerical Integration Strategies of PFR Dynamic Models with Axial Dispersion and Variable Superficial Velocity: The Case of CO_2 Capture by a Solid Sorbent. *Heliyon* **2019**, *5* (9), e02040.
(65) Stanmore, B. R.; Gilot, P. Review-Calcination and Carbonation of Limestone during Thermal Cycling for CO_2 Sequestration. *Fuel Process. Technol.* **2005**, *86* (16), 1707−1743.
(66) Zhou, Z.; Xu, P.; Xie, M.; Cheng, Z.; Yuan, W. Modeling of the Carbonation Kinetics of a Synthetic CaO-Based Sorbent. *Chem. Eng. Sci.* **2013**, *95*, 283−290.
(67) Di Felice, L.; Foscolo, P. U.; Gibilaro, L. CO_2 Capture by Calcined Dolomite in a Fluidized Bed: Experimental Data and Numerical Simulations. *Int. J. Chem. React. Eng.* **2011**, *9* (1), No. 2584, DOI: 10.1515/1542-6580.2584.

https://dx.doi.org/10.1021/acs.iecr.9b05383
Ind. Eng. Chem. Res. XXXX, XXX, XXX−XXX